



Universiteit
Leiden
The Netherlands

Chemical biology of glucosylceramide metabolism fundamental studies and applications for Gaucher disease

Oussoren, S.V.; Oussoren S.V.

Citation

Oussoren, S. V. (2017, September 28). *Chemical biology of glucosylceramide metabolism fundamental studies and applications for Gaucher disease*. Retrieved from <https://hdl.handle.net/1887/55842>

Version: Not Applicable (or Unknown)

License: [Licence agreement concerning inclusion of doctoral thesis in the Institutional Repository of the University of Leiden](#)

Downloaded from: <https://hdl.handle.net/1887/55842>

Note: To cite this publication please use the final published version (if applicable).

Cover Page



Universiteit Leiden



The handle <http://hdl.handle.net/1887/55842> holds various files of this Leiden University dissertation

Author: Oussoren, Saskia

Title: Chemical biology of glucosylceramide metabolism : fundamental studies and applications for Gaucher disease

Date: 2017-09-28

Stabilization of
glucocerebrosidase
by active-site occupancy

Stabilization of glucocerebrosidase by active-site occupancy

Based on

Fredj Ben Bdira^{a*}, Wouter W. Kallemeijn^{b*}, Saskia V. Oussoren^b, Saskia Scheijf^c, Boris Bleijlevens^c, Bogdan I. Florea^d, Cindy P. A. A. van Roomen^c, Roelof Ottenhoff^c, Marielle J. F. M. van Kooten^a, Marthe T. C. Walvoort^d, Martin D. Witte^d, Rolf G. Boot^b, Marcellus Ubbink^a, Herman S. Overkleeft^d, Johannes M. F. G. Aerts^{b,c}

^aDept. of Macromolecular Biochemistry, LIC, Leiden University

^bDept. of Medical Biochemistry, LIC, Leiden University

^cDept. of Medical Biochemistry, AMC, University of Amsterdam

^dDept. of Bio-organic Synthesis, LIC, Leiden University

ACS Chem Biol. 2017 May 22.
doi: 10.1021/acscchembio.7b00276.

Abstract

Glucocerebrosidase (GBA) is a retaining lysosomal β -glucosidase degrading glucosylceramide. Its deficiency results in Gaucher disease (GD). We examined the effects of active site occupancy of GBA on its structural stability. For this we made use of cyclophellitol-derived activity-based probes (ABPs) binding irreversibly to the catalytic nucleophile E340 and for comparison the potent reversible inhibitor, isofagomine. We demonstrate that cyclophellitol ABPs improve GBA stability *in vitro* as revealed by thermodynamic measurements (T_m increase by 21 °C) and its extreme resistance to tryptic digestion. The stabilizing effect of cell-permeable cyclophellitol ABPs is also observed in intact cultured cells containing wildtype, N370S GBA (labile in lysosomes) and L444P GBA (impaired ER folding): all showing marked increases in lysosomal forms of GBA molecules upon exposure to ABPs. The same stabilization effect is observed for endogenous GBA in liver of wild-type mice injected with cyclophellitol ABPs. Similar stabilization effects, as for ABPs, were also noted at high concentrations of the reversible inhibitor isofagomine. In conclusion, we provide evidence that the increase in GBA cellular level by ABPs and reversible inhibitors is in part caused by their ability to stabilize GBA folding and hence increased resistance against breakdown by lysosomal proteases. These effects are more pronounced in the case of the amphiphilic ABPs, presumably due to their high lipophilic potential, which may promote further structural compactness of GBA through hydrophobic interactions. Our study provides further rationale for the design of chaperones for GBA to ameliorate Gaucher disease.

Introduction

The lysosomal β -glucosidase glucocerebrosidase (GBA) cleaves glucosylceramide, an essential step in turnover of cellular glycosphingolipids^{1,2}. GBA is co-translationally translocated into the ER where it acquires four *N*-linked glycans³. After removal of its signal peptide, the 495 amino acid polypeptide completely folds and subsequently binds to the triple helical structure in the apical region of the integral membrane protein LIMP-2 (lysosome integral membrane protein 2, encoded by the *Scarb2* gene), and containing trafficking information in its cytoplasmic tail^{4,5}. Complexed to LIMP2, GBA is transported through the Golgi apparatus where its glycans are converted into complex-type structures⁶. The GBA-LIMP2 complex is routed to late endosomes/lysosomes where GBA dissociates as a result of local acid pH^{5,7}.

GBA belongs to family 30 of glycoside hydrolase clan A (www.cazy.org), hence its structural topology displays a typical $(\alpha/\beta)_8$ TIM barrel fold which forms the catalytic domain, a β -sheets domain and an immunoglobulin like domain, which interacts tightly with the catalytic domain, where few loops are located in the proximity of the enzyme active site⁸. These later seem to adopt multiple conformations, indicating their structural flexibility, presumably reflecting their crucial role in the enzyme conformational stability and/or its substrate turnover⁹. The inspection of GBA crystal structure in complex with NN-DNJ (PDB code:2V3E) shows that the binding site of the enzyme is formed by a hydrophilic glycon binding pocket, where the sugar ring of the inhibitor is accommodated forming multiple hydrogen bonds with its surrounding residues. In addition to the presence of an aglycon binding pocket formed by a narrow hydrophobic channel where the aliphatic tail of the inhibitor resides and forms a cluster of hydrophobic interactions with residues Leu241, Phe246, Tyr313, Leu314, and Tyr244¹⁰.

Deficiency of GBA results in Gaucher disease (GD, OMIM #203800)¹¹. At present more than 200 mutations in the *Gba* gene have been linked with GD, and next to truncations and splicing defects, several hundred amino acid substitutions in GBA have been shown to cause GD¹². Substitutions in the folding domain positioned far away from the catalytic site proved to destabilize GBA structure, hence decreasing its half-life within the cell. For instance, the substitution L444P in GBA causes faulty folding of most enzyme molecules in the ER and subsequent proteasomal degradation¹³. Homozygosity for L444P GBA nearly always leads to a severe neuronopathic course of GD, albeit with great individual variability in onset and progression¹¹. Premature degradation may also occur in the case of GBA molecules with mutations in the catalytic domain. In fact, quite many of the documented mutations in GBA lead to defective folding and reduced transport to lysosomes¹⁴. An exception is the N370S GBA substitution, the prevalent *Gba* mutation among Caucasians GD patients. The amino acid substitution is in a loop close to the catalytic pocket and found to affect pH optimum and kinetic parameters such as affinity for substrate and inhibitors¹⁵⁻¹⁹. The intralysosomal stability of N370S GBA is also reduced^{15,16,19}. The survival of wildtype GBA in lysosomes is already relatively short ($t_{1/2}$ ~24-36 hours), at least in cultured cells. The intralysosomal proteolytic breakdown of GBA is known to be mediated by cysteine proteases as suggested by its inhibition by leupeptin²⁰.

The major symptoms of GD are caused predominantly by the abnormal accumulation of glucosylceramide in lysosomes of tissue macrophages^{21,22}. Lysosomal accumulation of glucosylceramide induces a multi-system disorder with various symptoms such as hepatosplenomegaly, cytopenia and bone disease¹¹. Severely affected GD patients also develop neurological symptoms and GBA abnormalities have been recognized as risk factor for developing α -synucleinopathies²³. Enzyme replacement therapy (ERT), chronic intravenous administration of macrophage-targeted recombinant human GBA²⁴, markedly improves visceral symptomatology in GD patients, but the inability of the infused enzyme to pass the blood-brain barrier prohibits prevention and correction of neurological manifestations²⁵. An alternative treatment might be offered by so-called pharmacological chaperones that promote folding and stabilize the fold of (mutant) GBA through interacting with its catalytic site^{26–29}. These preferably brain-permeable, small compounds should promote folding of (mutant) GBA in the endoplasmic reticulum, resulting in increased transport of GBA to the lysosome^{26–29}. Additionally, pharmacological chaperones might also stabilize GBA intra-lysosomally¹⁵. Whether the latter is clinically beneficial is debated, since pharmacological chaperones that interact with the active site of GBA will intrinsically also inhibit its enzymatic activity. We wanted to address the question whether occupancy of the binding pocket of GBA may promote its protection against proteolytic degradation in lysosomes.

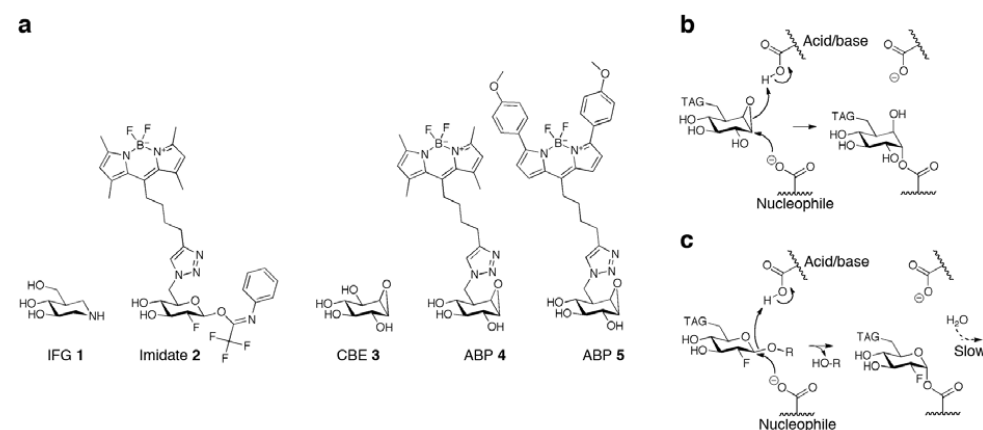


Figure 1. Inhibitors and reaction mechanism. (a) Structure formulas of competitive, reversible inhibitor isofagomine (IFG **1**), semi-irreversible inhibitor 2-deoxy-2-fluoro- β -D-glucopyranosyl-2-fluoro- β -D-glucopyranosyl-N-phenyltrifluoroacetimidate³⁰ (imidate **2**) and irreversible inhibitors conduritol β -epoxide (CBE **3**) and cyclophellitol β -epoxide type ABP **4** (MDW933, green fluorescent) and β -epoxide type ABP **5** (MDW941, red fluorescent)³². (b) Irreversible binding mechanism of β -epoxide type ABPs to the nucleophile of GBA via its double-displacement mechanism. (c) Hydrolysis of imidate **2**, and the temporary trapping of the glycosylated nucleophile adducts of GBA.

In the present study, we first examined pure recombinant glucocerebrosidase regarding stabilizing effects of cyclophellitol-type activity-based probes (ABPs, figure 1a) that permanently bind to the catalytic nucleophile E340 of GBA by utilizing its retaining double-displacement mechanism (figure 1b). These ABPs are β -glucose configured cyclophellitols with attached to the C6 a spacer with hydrophobic green- or red fluorescent BODIPY-moieties (MDW933 **4**, MDW941 **5**, figure 1a)^{30,31}. These amphiphilic compounds are supposed to mimic the natural substrate of GBA and bind both its glycon and aglycon binding pockets. We also used CBE **3** as a small hydrophilic covalent inhibitor that is supposed to occupy only the glycon binding pocket of GBA binding site. These mechanism based inhibitors take benefit from the first step of GBA catalysis reaction to trap the enzyme in its intermediate state forming an adduct complex, thus providing a valuable tool to dissect the contribution of each compound moiety into the stabilization mechanism by binding site occupancy on GBA.

We also examined the effect of 2-deoxy-2-fluoro- β -D-glucopyranosyl-2-deoxy-2-fluoro- β -D-glucopyranosyl-N-phenyltrifluoroacetimidate (imidate **2**, figure 1a)³² which forms a transient glycosyl-enzyme intermediate (figure 1c). For comparison, we studied the effect of the potent reversible competitive GBA inhibitor IFG **1** which has an *in vitro* IC₅₀ ~30 nM at pH 5.2 and 5 nM at pH 7.0²⁷. All inhibitors, most prominently the amphiphilic ABPs, **4** and **5**, improved stability of GBA and its proteolysis resistance *in vitro* and *in vivo* presumably promoted by their lipophilic tails that occupy the protein aglycon binding pocket, thus “inducing” a more rigid conformation of the protein trough hydrophobic interactions. Similar beneficial action on the stability and proteolysis resistance of GBA wildtype, N370S and L444P in cultured cells were observed. Marked increases in GBA tissue level were also noted for liver of mice infused with cyclophellitol ABPs. The stabilizing effects of the hydrophilic inhibitors IFG **1**, CBE **3** and the semi-reversible fluorosugar imidate **2** were less pronounced, suggesting that permanent occupancy of the glycon and aglycon binding pockets of GBA leads to a superior stabilization effect. The various investigations are here described and the implications are discussed.

Results

Structural stability and flexibility of GBA: impact of pH and glycomimetic ligands

During its life cycle glucocerebrosidase is exposed to a broad range of pH values, from neutral pH in the ER to increasingly acid pH in endosomes and lysosomes (pH 6.5 > pH 4.5–5.0). Therefore, we first investigated the effect of both acid and neutral pH on the structural stability of purified recombinant GBA (rGBA, imiglucerase) by monitoring its thermal unfolding, using circular dichroism. The temperature dependence of rGBA secondary structure at 222 nm was recorded by applying a temperature gradient from 30–80 °C with a heating rate of 1 °C/min (figure 2a). The obtained rGBA melting curve at pH 7.4 shows an apparent T_m value of 57 °C. On the other hand, its melting temperature increased at pH 5.2 with 4 °C to an apparent T_m value of 61 °C. This observed T_m increase at acidic pH is in

agreement with the previously reported measurements by differential scanning calorimetry^{15,33,34}. Next, we investigated the effect of isothermal incubation at different pH on the activity of rGBA, and whether this was time-dependent. For this purpose, rGBA was firstly incubated for different lengths of time intervals at 37 °C in 150 mM Mcllvaine buffer with a pH of 5.2 or 7.4. Residual activity of rGBA was measured with 4MU- β -D-Glc substrate in 150 mM Mcllvaine buffer, pH 5.2 (figure 2b). The obtained data indicate that rGBA preserves its activity under acidic conditions, whereas at pH 7.4 its activity is lost in a time-dependent manner with a half-life of 30 min.

The noted loss of rGBA activity at pH 7.4 could be due to loss of the enzyme's native fold, apparently due to an irreversible process since the remaining activity was measured at pH 5.2. To substantiate this explanation, we performed a trypsin-limited proteolysis reaction to probe the pH effects on rGBA rigidity. For this, rGBA was treated with trypsin in 150 mM Mcllvaine buffer at pH 5.2 or 7.4 and the tryptic events were analyzed every 10 min by SDS-PAGE (figure 2c). At pH 5.2, rGBA shows resistance to tryptic digestion over the course of the reaction, while at pH 7.4, rGBA is more sensitive to trypsin digestion, with about 40 % degraded within 60 min. Of note, a tryptic fragment of 34 kDa appears during proteolysis and it persists over the course of the reaction events, which may point to a structured and rigid, nicked domain of rGBA (figure 2c, *arrow*). Mass spectrometry was used to tentatively identify the trypsin cleavage site in GBA. It suggested that the cleavage site position could be after Lys233 (UniProt:P04062, fasta sequence, see supplemental figure S3) within the polypeptide sequence VNGK_GSL located in a loop close to the active site. This cleavage site seems to be more accessible to trypsin digestion at neutral pH and more protected at acidic pH. Seemingly, due to the different adopted conformation of rGBA under these experimental conditions (figure 2d).

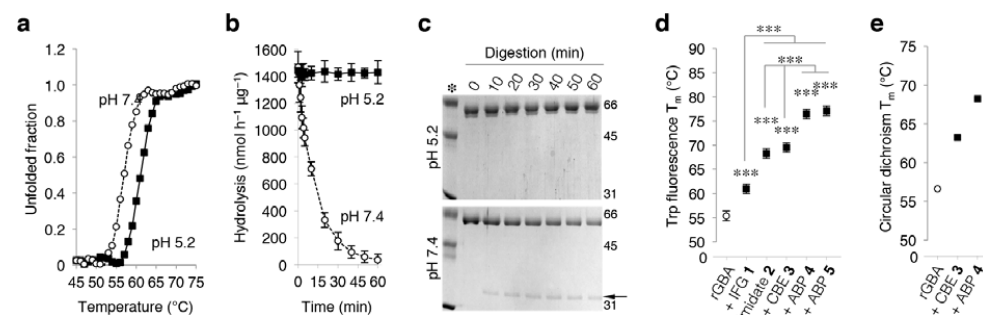


Figure 2. pH affects the rGBA structure. (a) rGBA melting curve at pH 5.2 (*closed squares*) and pH 7.4 (*open circles*) as determined by circular dichroism. (b) Time-dependent decay of rGBA activity at pH 5.2 (*closed squares*) and pH 7.4 (*open circles*), as determined by hydrolysis of 4MU- β -D-Glc substrate at pH 5.2. Data are average of duplicates \pm SD. (c) Coomassie brilliant blue (CBB) staining of time-dependent, tryptic digestion of rGBA with a trypsin/rGBA ratio of 1/10 (w/w) at pH 5.2 and 7.4 (*top, bottom*, respectively). Arrow highlights the 35 kDa tryptic

fragment. (d) Melting temperature (T_m) determined by tryptophan fluorescence of rGBA in absence (control) or presence of saturating inhibitor concentrations of IFG **1**, imidate **2**, CBE **3**, β -epoxide ABPs **4** and **5**. Statistical analysis of $n = 3$ experiments, two-way ANOVA, $p < 0.001^{***}$. (e) T_m determined by circular dichroism of rGBA in absence or presence of saturating inhibitor concentrations of **3** and **4**. Statistical analysis of $n = 2$, two-way ANOVA, $p < 0.001^{***}$.

Thermal stability of rGBA: impact of glycomimetic ligands

The effects of the competitive inhibitor isofagomine (IFG **1**), the semi-irreversible inhibitor 2-deoxy-2-fluoro- β -D-glucopyranosyl-trichloroacetimidate (imidate **2**) and the irreversible inhibitors conduritol β -epoxide (CBE **3**) and lipophilic cyclophellitol β -epoxide type ABPs **4/5** on thermal stability of rGBA were investigated at pH 5.2, mimicking lysosomal conditions. For this purpose, rGBA was incubated with saturating concentrations of inhibitors for 1 h at 37 °C and next gradually heated whilst measuring tryptophan fluorescence^{35,36}, which decays as a result of tertiary structure unfolding. As depicted in figure 3a, IFG **1** increased the T_m of rGBA (55.2 °C) by +5.6 °C, **2** by +12.9 °C, irreversible inhibitor **3** by +14.1 °C and ABPs **4** and **5** by +21.0 and +21.7 °C, respectively. Another analysis of biophysical stability was performed by circular dichroism³⁷. rGBA without inhibitors was compared to enzyme saturated by **3** and β -epoxide **4** (figure 3a). The calculated melting temperatures of rGBA preparations follow a similar trend as observed with tryptophan fluorescence decay (figure 3b). Again, β -epoxide **4** is found to exert the most prominent stabilization of rGBA.

Glycomimetic ligands influence the intrinsic fluorescence of GBA.

We next exploited the twelve tryptophan-residues present in GBA to probe the effects of ligand binding on the general folding of GBA. Notably, Trp178 and Trp381 are in close proximity of the substrate binding pocket, and residues Trp348 (loop 2), Trp393 (loop 3) reside on the protein surface, while the other Trp residues are buried into the hydrophobic core of the protein⁸. For this purpose, rGBA emission spectra were acquired by exciting tryptophan residues at 295 nm and recording the emission spectrum by scanning from 300–450 nm, in the presence or absence of various (ir)reversible inhibitors (figure 3c). In its free form, rGBA exhibits a maximum emission of 336.5 nm (similar as previously reported³⁶). A slight blue shift of the spectrum by 2 nm was observed upon complex formation with CBE **3** with a maximum emission at 334.5 nm, reflective of a more hydrophobic environment of the Trp residues within the complex state (see figure 2c). rGBA exhibits a slightly larger blue shift when bound to ABPs **4** and **5**, with emission maximums of 333 nm. These data suggest that CBE **3** and ABPs **4/5** cause changes in rGBA folding, with higher effects of the latter ABPs presumably promoted by their lipophilic tails. Serendipitously, the blue shifts induced by ABP **4** and **5** were concomitant with fluorescence quenching. As ABP **4** and **5** contain a BODIPY fluorescence moiety (green and red fluorescent, respectively), we speculate that part of intrinsic GBA tryptophane-emitted fluorescence is transferred to these fluorophores through

an intrinsic FRET (iFRET) mechanism³⁸. To test this, the fluorescence spectra of ABP 4- and ABP 5-labeled rGBA were acquired by exciting at 295 nm and extending the scanning range to 700 nm. Indeed, two peaks appear at a maximum emission of 515 nm and 610 nm, which represent the maximum emission for both ABP-incorporated BODIPYs (figure 3d). This iFRET mechanism is also supported by the overlaps between rGBA and ABPs emission spectra (Supplemental Figure S1).

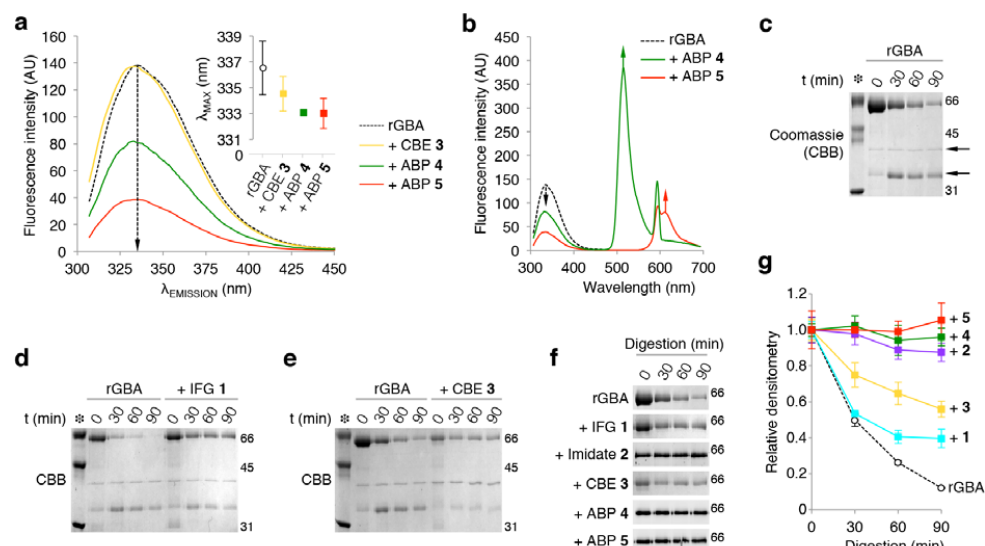


Figure 3. rGBA conformational changes monitored by intrinsic fluorescence. (a) rGBA fluorescence spectra with λ_{EX} 295 nm in the absence of additives (control, blue) with a maximum λ_{EM} 335 nm, in complex with CBE 3 (yellow) with a maximum λ_{EM} 333 nm, with ABP 4 (green) with a maximum λ_{EM} 332 nm and with ABP 5 (red) with a maximum λ_{EM} 331 nm. (b) rGBA fluorescence spectra showing the fluorescence quenching by ABP 5 (red) with the appearance of an emission peak at 610 nm and ABP 4 (green) with the emerge of an emission peak at 515 nm. All the measurements were done in 10 mM phosphate buffer, 150 mM NaCl pH 7.4. (c) Time course analysis of rGBA trypsin digestion. Arrows highlight the 40 and 35 kDa tryptic fragments. (d, e) Time course analysis of rGBA tryptic digestion in complex with IFG 1 and CBE 3. (f) rGBA band intensities over the course of tryptic digestion stained by CBB or detected by ABP-emitted fluorescence. (g) Quantification of rGBA band densitometry over the course of tryptic digestion in the absence and in the presence of ABP 4 (green), imidate 2 (magenta), ABP 5 (red), CBE 3 (yellow) and IFG 1 (blue). Duplicate quantification \pm SD.

Glycomimetic ligands variably rigidify the GBA structure.

Protein stabilization by ligands is generally paired with protein rigidification, due to new hydrogen-bond formation, or due to the formation of new clusters of hydrophobic interactions³⁹. From the data presented above, we speculate that there is a correlation between the induced conformational changes by the ligand and the thermodynamic stabilization of GBA. We next investigated whether interactions with (ir)reversible inhibitors stabilize GBA by rigidification *in vitro*, by analyzing their effect on the ability of trypsin to digest rGBA. As can already be seen in figure 2c, purified rGBA is rapidly digested by trypsin, forming two major fragments (\sim 35 and \sim 40 kDa), which remain mostly intact over the course of the experiment. After 90 min, \sim 10 % of intact rGBA remains. Presence of IFG 1 or CBE 3 increased resistance against tryptic digestion, with 50 % of rGBA remaining intact (figure 3 e,f). Imidate 2 and ABPs 4 and 5 exert prominent effects on the sensitivity of rGBA for tryptic digestion (figure 3 e,f), as such that within 90 min no degradation was observed. These ABPs have long hydrophobic tails of 15–18 Å, which give them a high lipophilic potential, suggesting that GBA rigidifies when interacting with these lipophilic ABPs, plausibly also shielding GBA's hydrophobic core and locking flexible loops in the vicinity of the active site through a cluster of hydrophobic interactions. Altogether, these observations match the increases in melting temperature (figure 3a–b). Of note, the amphiphilic inhibitors 4 and 5 show the lowest IC_{50} values regarding inhibition of GBA enzymatic activity, reflecting their highest binding affinity (see figure 1).

Lipophilic ABPs 4 and 5 stabilize GBA in macrophages and living mice.

As ABPs 4 and 5 exerted the strongest effect on rGBA stability *in vitro*, we assessed their influence on the enzyme *in situ*. Hence, human monocyte-derived macrophages were cultured with 100 nM ABP 5, completely labeling all active GBA molecules (*in situ* $IC_{50} \sim$ 10 nM). After a continuous pulse for up to 192 h (8 days), *in situ* ABP 5-labeled GBA was detected by fluorescence scanning (figure 4a). ABP 5 labeled various molecular weight forms of GBA in the range 58–66 kDa, stemming from modifications in the enzyme's N-linked glycans⁴⁰. Earlier investigations have revealed that the 58 kDa form of GBA is formed inside lysosomes as the result of trimming of N-linked glycans by local glycosidases⁴⁰. As seen in figure 4a, the mature 58 kDa form of GBA accumulates when the enzyme is labeled with 5. This finding suggests that ABP-labeling stabilizes GBA against proteolytic degradation in lysosomes, and does not prohibit the N-glycan modifications by lysosomal glycosidases.

To further examine the stabilizing effect of ABPs on GBA *in situ*, we analyzed the fate of exogenous, unlabeled rGBA and identical enzyme pre-labeled with ABP 4 following uptake by human monocyte-derived macrophages (figure 4b). The ABP 4-labeled enzyme was stable after uptake for at least 48 hours, sharply contrasting with the rapid breakdown of unlabeled rGBA (figure 4c).

Next, we infused mice intravenously with 1 nanomole ABP 4 which subsequently labeled endogenous GBA in various tissues^{31,32,41}. In the livers of treated animals, sacrificed six weeks post ABP-administration, ABP 4-labeled GBA could still be detected (figure 4d). The

amount was around ~35 % of that in the livers of animals that were sacrificed 24 hours after infusion of an identical dose of ABP 4. This suggests again that ABP-labeling markedly stabilizes GBA *in vivo*, since the half-life of unlabeled GBA is reported to be around 32–48 hours^{18,20}.

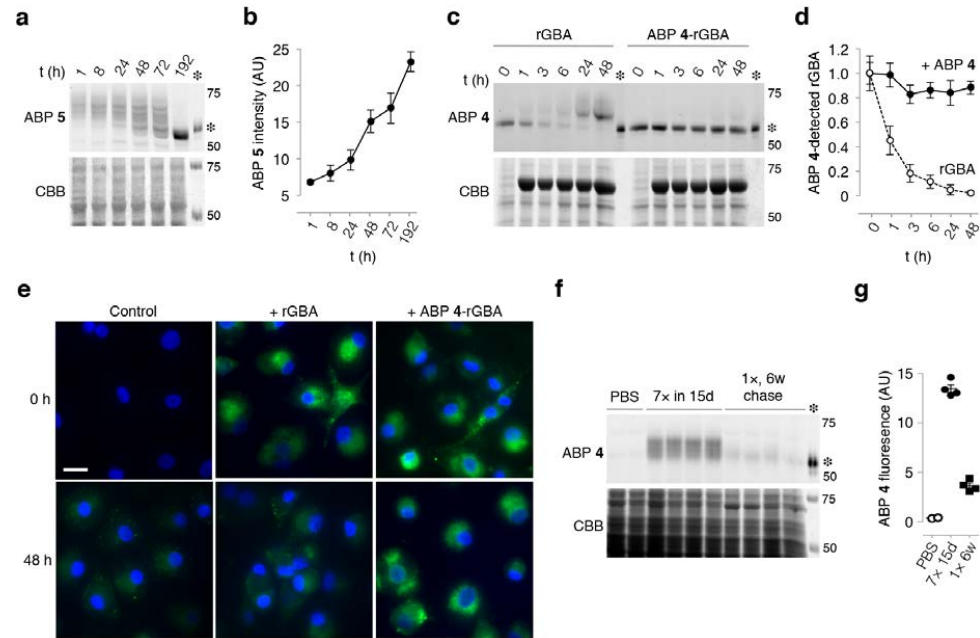


Figure 4. *In situ* labeling of GBA with ABP 4/5. (a) Continuous labeling of human monocyte-derived macrophage GBA with ABP 5 (*top panel*) and Coomassie staining of protein input (CBB, *bottom*). (b) Densitometry of ABP 5-emitted fluorescence, corrected to CBB (mean of duplicate quantification, \pm SD). (c) Chase of ABP 4 (pre-) labeled rGBA (imiglucerase) taken up by CBE pre-treated human monocyte-derived macrophages (*top*) and CBB (*bottom*). (d) Densitometry of ABP 4-emitted fluorescence, corrected to CBB, with rGBA (*open circle*) and ABP 4-labeled rGBA (*closed square*), mean of duplicate quantification \pm SD. (e) Fluorescence micrographs of chase in (c), of control (*left*), and cells treated with unlabeled rGBA (*middle*) and ABP 4-labeled rGBA, after 0 and 48 h (*top, bottom, respectively*). Unlabeled rGBA was labeled 30 min prior to fixation with 10 nM ABP 4. Scale-bar represents 25 μ m. (f) Chase of murine hepatic GBA of animals treated either with vehicle or ABP 4 during 15 days (7 injections), or a single dose 6 weeks prior sacrifice (*top panel*) and CBB (*bottom*). (g) Densitometry of ABP 4-emitted fluorescence, corrected to CBB, with untreated (*open circle*), ABP 4 repeatedly (*closed diamond*) and single dose (*closed square*), mean of duplicate quantification \pm SEM. All gels contain 50 fmol equimolar ABP 4- and 5-labeled ~58 kDa imiglucerase (*asterisk*) as positive control.

Lipophilic ABPs 4 and 5 increase GBA in fibroblasts by protection against lysosomal proteolysis.

To assess whether the accumulation of ABP 4-labeled 58 kDa GBA stems from a reduced susceptibility towards lysosomal proteases, we treated confluent human control fibroblasts for 3, 5, 7, 9 or 12 days with the cysteine-cathepsin inhibitor leupeptin²⁰. After harvesting the cells, GBA present in lysates of control cells and leupeptin-exposed cells was *in vitro* labeled with excess ABP 4. As shown in figure 5a, the amount of green 4-labeled GBA in untreated control cells increased slightly with culture time (*top row*). The incubation of cells with leupeptin caused a prominent accumulation of ~58 kDa active GBA over time (*second row*)²⁰.

Next, we incubated cells with ABP 5. The inhibitor treatment induced a prominent time-dependent accumulation of ABP-labeled GBA (*third row, figure 5a*). The increase in *in situ* ABP 5-labeled GBA was slightly further enhanced in cells co-incubated leupeptin (*fourth row*), suggesting 5-labeled GBA is still prone to some degree of proteolysis within lysosomes (figure 5a). The quantification of GBA levels is shown in figure 5b, indicating that *in situ* stabilization of GBA by leupeptin and ABP 5 is at least partially overlapping.

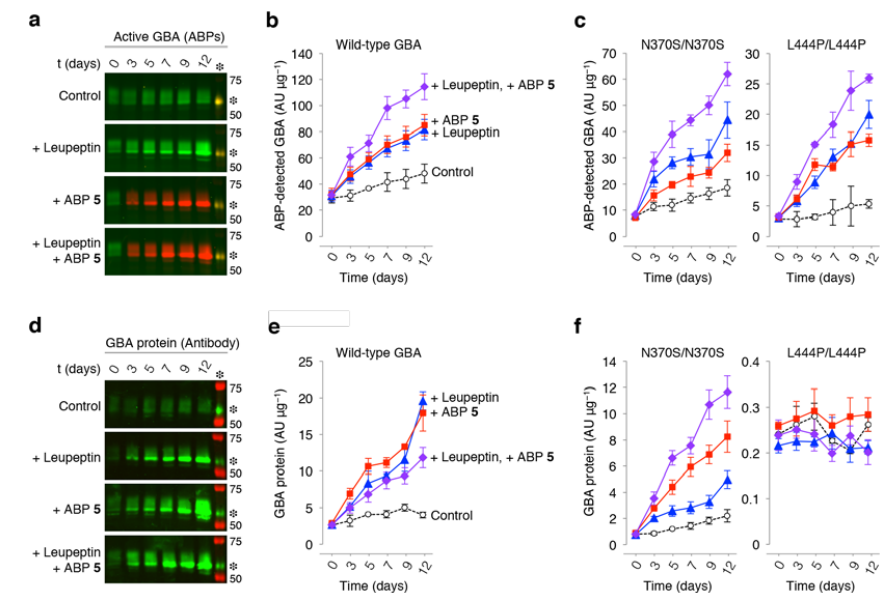


Figure 5. *In situ* stabilization of GBA by ABP 5 and leupeptin. Wild-type GBA fibroblasts incubated with leupeptin, ABP 5 (*red*), or both for the indicated length of time. (a) GBA levels in untreated fibroblasts (*top row*) and cells incubated with leupeptin (*second row*), visualized *in vitro* with ABP 4 (*green*). Labeling of GBA in cells *in situ* with ABP 5 (*red, third row*) and in combination with leupeptin (*bottom row*). Equal green and red fluorescence yields yellow overlay; fluorescence was calibrated with 50 fmol equimolar green ABP 4- and red ABP 5-labeled imiglucerase present on each SDS-PAGE gel (*asterisk*). (b) Quantification of ABP-emitted fluorescence from *in vitro* ABP 4-labeled controls (*open black circles*) and leupeptin

(blue triangles), and *in situ* ABP 5-labeled GBA (red squares), and in combination with leupeptin (purple diamonds). Data as mean of $n = 2$, \pm SD. (c) Quantifications of ABP-fluorescence as observed in N370S and L444P Gaucher fibroblasts, *vide supra*. (d) Detection of GBA protein (green) with Western immunoblotting of gels depicted in a (molecular weight ladder in red), with quantification in (c) and identical analysis of N370S and L444P Gaucher fibroblasts, *vide supra*. All data expressed as average of $n = 2$, \pm SD.

Lipophilic ABPs 4 and 5 increase mutant GBA molecules in GD fibroblasts.

In fibroblasts from a homozygous N370S GBA Gaucher patient and a homozygous L444P GBA Gaucher patient, similar stabilizing effects of ABP on enzyme were observed (figure 5c). Both fibroblast cell lines contained less active GBA compared to the control fibroblasts. Incubation of the cells with leupeptin and ABP 5 resulted in stabilization of GBA, more prominent (6- to 8-fold) compared to that seen for GBA in wild-type cells (about 3-fold) (compare figure 5b and 5c). Exposure of both Gaucher fibroblast cell lines to the combination of ABP 5 and leupeptin further increased the stabilizing effect, again partially overlapping (Figure 5c, see supplemental information for original data). Total GBA protein in cell lysates was also visualized by Western blot using GBA-specific antibody 8E4^{42,43} (figure 5d; *corresponding quantification in figure 5e*). Again, prominent stabilization of ~58 kDa GBA was noted with ABP 5 and/or leupeptin in the case of wild-type cells and N370S GBA Gaucher fibroblasts (figure 5f). Comparable analysis of L444P GBA Gaucher fibroblasts was unfortunately not reliable due to the very low quantities of GBA protein. Overall, these findings suggest that the stabilizing effect of ABP 5 is partially caused by protection against breakdown by lysosomal proteases. This effect is specific since the lysosomal glycosidases processing GBA to its 58 kDa form appear to be not inhibited.

The reversible inhibitor IFG and semi-irreversible inhibitor 2 were found to augment GBA to a lesser extent in fibroblasts. Confluent wild-type and homozygous N370S GBA fibroblasts were treated for 12 days with 0–100 μ M of 1. After harvesting, cell lysates were labeled with excess green ABP 4 to visualize residual active GBA molecules (Supplemental information Figure S2). A stabilizing effect of IFG 1 became only evident at concentrations greater than 10 μ M, being maximal at 100 μ M (*the highest concentration tested*). Western-blot analysis of the same experiment, rendered a similar result (Supplemental information figure S2). The semi-irreversible inhibitor ABP 2 comparably augmented GBA in wild-type and N370S/N370S GD fibroblasts (supplemental information figure S2). The findings made for imidate 2 treatment were confirmed by Western blot analysis (see supplemental information figure S2).

Discussion

In recent years attention has been paid to the design and synthesis of chemical chaperones for GBA. Reviews by Benito *et al.*²⁸ and Jung *et al.*⁴⁴ cover some of the classes of glycomimetics currently under investigation as GBA chaperones. Many of these are reversible competitive, or mixed-type, inhibitors of GBA. The most well studied chemical chaperone so far has been IFG 1, which was the subject of several pre-clinical studies as well as a clinical study that did not meet the full expectation. Ambroxol^{45–48}, a weak, mixed-type inhibitor of GBA, has been found to augment the enzyme in cultured GD patient cells and following oral administration to patients. Impressive reductions in spleen and liver volumes, as well as the GD biomarker chitotriosidase, have been documented^{47,49}. The beneficial effects of chemical chaperones on GBA in cultured cells are generally attributed to improved chaperone-assisted folding of GBA in the endoplasmic reticulum. Our present investigation suggests an additional beneficial mode of action of inhibitors. i.e. The contribution of hydrophobic interactions of GBA binding pocket occupancy into the enhancement of its structural stability and protection against intralysosomal proteolytic degradation.

The evidence for this notion stems from *in vitro* and *in vivo* experiments testing GBA stabilization by inhibitors. Thermodynamic measurements with pure GBA suggested firstly that, correlating with affinity of inhibition, all inhibitors tested stabilized enzyme. A modest stabilization of GBA was observed for small hydrophilic compounds IFG 1 and conduritol β -epoxide 3. The lipophilic fluorosugar 2 and β -epoxides 4/5 equipped with hydrophobic fluorophores cause a more dramatic increase of melting temperature up by 21 °C. Next, we analyzed using intrinsic fluorescence the conformational changes of GBA *in vitro* following interaction with inhibitors. Upon complex formation with CBE 3 GBA presents a slight shift toward the blue region of its fluorescence spectra, an indication for a conformation change, possibly resulting from orientation adjustments of indole groups toward a more hydrophobic environment. A higher shift toward the blue region was observed when the protein is in complex with lipophilic ABPs 4 and 5. Presumably their lipophilic tails provoke further conformational changes in which the indole groups of a tryptophan experience extra hydrophobicity. Of note, equipment of cyclophellitol and cyclophellitol-aziridine with hydrophobic fluorophore tags markedly increases their affinity for GBA^{30,31}. Along the same line, Vocadlo and co-workers developed an elegant fluorescence-quenched substrate for GBA for which they exploited the fact that GBA accommodates the hydrophobic ceramide moiety of glucosylceramide and is known to tolerate a hydrophobic modification to the 6-position of glucose⁵⁰. The designed high-affinity fluorescence-quenched substrate harbors a fluorophore attached to the C6-glucose and the hydrophobic quencher to the anomeric site and to a certain extent mimics fluorosugar 2 and ABPs 4 and 5. This successful substrate design indicates again that the catalytic pocket of GBA in active state accommodates substrate with a hydrophobic modification. At present no crystal structure of GBA has been solved in the presence of the ABPs 2, 4 or 5. However, the crystal structure of GBA in complex with a lipophilic ligand (*N*-nonyl-DNJ, PDB code 2V3E) suggests that GBA loops 1 and 2 become structured and undergo interactions with the aliphatic tails of *N*-nonyl-DNJ, becoming more

closed and thermostable³⁴. Similarly, upon complex formation with the ABPs **2**, **4** and **5**, GBA becomes extremely protected against tryptic digestion, providing strong evidence of its structure rigidification. In the presence of hydrophilic compounds such as IFG **1** or CBE **3**, GBA behaves similarly to its free form, with a moderate enhancement of its tryptic resistance. These observations support the proposition of GBA rigidification by the lipophilic ligands, presumably through a cluster of hydrophobic interactions. Therefore, we presume that the observed differences of the stabilization mechanisms between the tested compounds are mainly due to the difference in their lipophilic potentials.

The predominant trypsin cleavage site in GBA free state is located in a loop (223-241 Uniprot:P04062 fasta sequence) close to the active site. In solution, this loop seems to be accessible for trypsin digestion by adopting a flexible conformation that fits within the protease catalytic site. As it is well known that protease cleavages site for a variety of proteins with solved crystal structure almost never occur in α -helices, but largely in flexible loops⁵¹. Interestingly sixteen mutations within this protein region were reported in human to decrease dramatically GBA stability and activity leading to severe symptoms of the disease. For instance, the substitution of L224F decreases GBA normal activity up to 4 % and increases its susceptibility to proteolytic degradation⁵². Another substitution V230E has a dramatic effect on GBA activity and presents in GD patient type 1⁵³. Single mutation G232E is present in patients suffering from Parkinson disease and this GBA variant preserve only 7 % of the wildtype normal activity⁵⁴. Moreover, substitution of G234E in GBA sequence has similar effect on Gaucher patients⁵⁵. The position of the latter mutation overlaps with what we found as a major trypsin cleavage site. Based on these findings, it is plausible that this particular region represents a hotspot for maintaining a correct folding of GBA catalytic domain. Upon complex formation with ABPs, this site becomes shielded against proteolytic degradation. Thus it is attractive to hypothesize that complexing the enzyme with ABPs **2**, **4** and **5** prevents GBA to become loose and locally flexible, improving its structural stability and resistance against proteolysis.

We recently noticed a similar stabilization mechanism for another retaining β -glucosidase, endoglycoceramidase II (EGCII) from *Rhodococcus sp*⁵⁶. The stability of EGCII was found to be improved by formation of covalent complexes with cyclophellitols substituted with hydrophobic moieties. The tested compounds seemed to have an induced fit mechanism effect on the protein flexible structure, which makes it adopting a more compact conformation. This was evidenced by the increase of EGCII melting temperature, its resistance against tryptic digestion, the observed changes in its ¹⁵N-¹H transverse relaxation optimized spectroscopy spectrum, and the decrease of its exposed hydrophobic surface to the solvent as determined by 8-anilino-1-naphthalenesulfonic acid fluorescence. Stabilization of EGCII conformation was correlated with the shape and hydrophobicity of the cyclophellitols substituents. The structural comparison between GBA and EGCII showed a remarkable overlaps of their glycon and aglycon binding pocket⁵⁶. Therefore, it will not be surprising if a similar stabilization mechanism of ABPs takes place in GBA case. Following the observed *in vitro* stabilization of GBA by inhibitors, we extended our study to living cells and mice. We

consistently noted that exposing cells (monocyte-derived macrophages, skin fibroblasts) and mice to cyclophellitol ABPs **4** or **5**, resulted in accumulation of GBA with a molecular weight of approximately 58 kDa, suggestive of a lysosomal localization. Co-incubation of fibroblasts with ABPs and leupeptin, a broad lysosomal cysteine protease inhibitor known to inhibit proteolytic breakdown of GBA, indicated that the stabilizing effect could indeed be partly ascribed to reduced breakdown

Our study reveals that irreversible inhibitors like cyclophellitol ABPs **4** and **5** potentially stabilize GBA molecules, but by virtue they are of no use in the treatment of GD patients. Although they provided a valuable tool to dissect the contribution of hydrophobic interactions into GBA stabilization and to selectively label the active form of GBA in cells. Fluoroglucosides, designed by Withers and co-workers⁵⁷, in theory may be more attractive as chaperones since they initially covalently bind to the catalytic nucleophile of a retaining glycosidase but are ultimately released again. A true therapeutic application of such compounds in patients will however offer the major challenge to dose the inhibitor adequately to reach concomitant beneficial effects in all tissues: under-dosing in a tissue will be without effect and over-dosing will cause undesired loss of degradative capacity. More relevant is the consideration that the natural substrate glucosylceramide assists in the stabilization of GBA in lysosomes. In such hypothetical scenario, intra-lysosomal GBA levels would be higher during high substrate flux, and *vice versa*, the prolonged absence of substrate would promote degradation of the enzyme. It will be of interest to examine whether reduction of glycosphingolipids in cells by inhibition of glucosylceramide synthase activity is associated with increased lysosomal turnover of GBA.

In conclusion, GBA is significantly stabilized through the dual occupancy of its glycon and aglycon binding pockets by amphiphilic inhibitors (see fig. S4), likely in part by promoting a global structural compactness of the enzyme associated with reduced susceptibility for proteolytic cleavage by lysosomal proteases. On the other hand, the single occupancy of the glycon binding pocket by small hydrophilic compounds seems to induce a local GBA structural rigidification as revealed by its *in vitro* and *in vivo* proteolysis susceptibility. Our findings reveal new insights into a pharmacological chaperone stabilization mechanism that could be further exploited in the design of new compounds to rescue GBA proteostasis in GD patients.

Materials & Methods

General methods.

The ABPs and isofagomine were synthesized as described earlier^{31,32,41}. Chemicals were obtained from Sigma-Aldrich if not indicated otherwise. Recombinant GBA (rGBA, imiglucerase) was obtained from Genzyme (Cambridge, MA, USA). Gaucher patients were diagnosed on the basis of reduced GBA activity and demonstration of an abnormal genotype. Fibroblasts were obtained with consent from donors. Cell lines were cultured in HAMF12-DMEM medium (Invitrogen) supplied with 10 % (v/v) FBS. Monoclonal anti-human GBA

antibody 8E4 was produced from hybridoma cells as described earlier⁴³. Buffy-coats were purchased at Sanquin Bloodbank (Amsterdam).

Cerezyme purification.

rGBA (imiglucerase) is supplied as a sterile white lyophilized powder in the presence of mannitol and polysorbate 80 NF as stabilizer substances. Thorough purification of rGBA from its additives was conducted by affinity chromatography using a Concanavalin A–Sepharose column, eluting with a 30 min gradient of 0–1 M mannoside in 150 mM Mcllvaine buffer (citric acid–Na₂HPO₄, pH 5.2). Next, an additional purification step was performed on pooled fractions using size exclusion chromatography (Superdex 75) and elution occurred either with 150 mM Mcllvaine buffer (citric acid–Na₂HPO₄, pH 5.2) or with 20 mM Tris–HCl, pH 7.4, supplemented with 150 mM NaCl. rGBA was concentrated Amicon Ultra-4 centrifugal filter devices (30 kDa cutoff) and kept at 4 °C for further experiments.

Limited proteolysis.

Tryptic digestion of purified rGBA with or without reversible or irreversible inhibitors was performed at 37 °C, either in 150 mM Mcllvaine buffer (pH 5.2 or 7.4) or in 20 mM Tris–HCl, pH 7.4, supplemented with 150 mM NaCl, and using a trypsin/rGBA ratio of 1/10 (w/w) as optimum condition for proteolysis. Digestions were stopped with cracking buffer (50 mM Tris–HCl, pH 6.8, supplemented with 1 % (w/v) SDS, 25 % (v/v) glycerol, 1 % (v/v) β-mercaptoethanol and 0.05 % (w/v) bromophenol blue), immediately followed by heating for 10 min at 100 °C. The tryptic digestion products (1.5–5 μg) were separated by SDS-PAGE and analyzed by Coomassie staining, or where stated, by fluorescence scanning (*see below*).

Tryptophan fluorescence.

rGBA (50 μM) was pre-incubated with 1 mM of IFG **1** or imidate **2**, 10 mM conduritol β-epoxide **3**, or 100 μM cyclophellitol ABP **4** or **5** in 150 mM Mcllvaine buffer (citric acid–Na₂HPO₄, pH 5.2, supplemented with 0.2 % (w/v) sodium taurocholate and 0.1 % (v/v) Triton X-100 for 3 h at 37 °C. Fluorescence decay curves were obtained by diluting to 1 μM rGBA-inhibitor complex in Nanopure H₂O, followed by determination of tryptophan fluorescence (λ_{EX} 295 nm, slit width 5 nm; λ_{EM} 345 nm, slit width 5 nm) whilst the sample temperature increased 1.5 °C per minute. Sample temperature was controlled *via* a PTP-1 Fluorescence Peltier System (Perkin-Elmer). We defined the inflection point of the temperature-induced decrease in tryptophan fluorescence intensity as the melting temperature (T_m). This value was determined by taking the minimum value of the first-derivative of the slope, at which the negative slope is maximal, using GraphPad Prism 5.1. The tryptophan emission fluorescence spectra was mapped using λ_{EX} 295 nm, slit width 5 nm, and scanning emission at λ_{EM} 300–470, slit width 5 nm (Cary Eclipse Fluorescence Spectrophotometer, Agilent Technologies). Samples comprised of 5 μM of purified rGBA with or without **3**, **4** or **5** in 10 mM potassium phosphate buffer (K₂HPO₄–KH₂PO₄, pH 7.4), supplemented with 150 mM NaCl. Spectral backgrounds were corrected and smoothed using

Cary Eclipse Fluorescence Spectrophotometer software. To obtain the different protein-inhibitors complexes, purified rGBA was pre-incubated with inhibitors in excess for 3 hours at 37 °C in 150 mM Mcllvaine buffer. After labeling, excess of irreversible inhibitors was removed *via* buffer exchange into 10 mM potassium phosphate buffer using Centriprep filter devices (30 kDa cutoff).

Circular dichroism.

Spectra were recorded on a Chirascan CD spectrometer (Applied Photophysics). Far-UV CD spectra were recorded from 180 to 300 nm in a 1 mm path length quartz cuvette (Hellma) at 20 °C at a concentration of ca. 10 μM. Spectra were collected for 0.5 s per data point at 0.5 nm step size (spectral bandwidth 1 nm) and were corrected for background signals. A Peltier element was used to control the sample temperature and allow ramping at 1 °C per minute. Intensity of the CD signal was monitored at various wavelengths (204, 215 and 235 nm). The unfolding transition point (T_m) of free purified rGBA at different pH (5.2 or 7.4) was measured by following the ellipticity signal decay at 222 nm by applying a heating rate of 1 °C/min, over a temperature gradient from 30–80°C in 10 mM potassium phosphate buffer (K₂HPO₄–KH₂PO₄, pH 5.2 or 7.4), supplemented with 150 mM NaCl). Obtained melting curves were fitted, and the T_ms were calculated using GraphPad Prism 5.1.

Enzyme activity assays.

The residual β-glucosidase activity associated with GBA was assayed at 37 °C by incubating samples with 3.75 mM 4-methylumbelliferyl-β-D-glucopyranoside (4MU-β-D-Glc) as substrate in 150 mM Mcllvaine buffer, pH 5.2, supplemented with 0.1 % (w/v) BSA, 0.2 % (w/v) sodium taurocholate, and 0.1 % (v/v) Triton X-100⁴². Time-dependent decay of rGBA activity was assessed by incubating rGBA for 0–60 min at 37 °C, and at various time points, the residual rGBA activity was assessed by adding substrate. Assays were stopped with excess NaOH-glycine (pH 10.3) and fluorescence was measured with a fluorimeter LS30 / LS55 (Perkin Elmer) using λ_{EX} 366 nm and λ_{EM} 445 nm.

Isolation and maturation of macrophages.

Buffy-coats were diluted into PBS supplemented with 0.1 % (w/v) BSA and heparin, subsequently layered on top of Lymphoprep gradient (Stemcell Technologies) and centrifuged at 1,000× *g* for 15 min at RT. After washing the PBMC pellets with PBS supplemented with 0.1 % (w/v) BSA, cells were centrifuged at 750× *g* for 10 min at RT, rinsed and repeated at 500× *g* for 5 min. Hereafter, the pellet was washed with aforementioned PBS, and centrifuged at 250× *g* for 10 min at RT. Then, monocytes were separated on a Percoll gradient. The resulting pellet was resuspended in 2.5 mL 60 % (w/v) SIP, layered with 5 mL 45 % (w/v) SIP and 2.0 mL 34 % (w/v) SIP), and centrifuged at 1750× *g* for 45 min at RT. The upper interface containing monocytes was washed thrice with aforementioned PBS, centrifuged at 500× *g* for 10 min and then twice at 500× *g* for 5 minutes. The cell fraction was then resuspended in RPMI with 1 % (w/v) human serum, the monocytes were counted with

trypan blue solution and 10^6 monocytes were seeded per well. After 1 h at 37 °C and 5 % (v/v) CO₂, non-adhering non-monocyte cells were washed away with aforementioned PBS and the adhering monocytes then were cultured in RPMI with 10 % (v/v) human serum for 7 days prior to experiment initiation.

Continuous β -epoxide ABP 5 pulse in human monocyte-derived macrophages.

Human monocyte-derived macrophages were switched to X-VIVO 15 medium (Lonza) lacking human serum, and continuously pulsed with 100 nM β -epoxide ABP 5. After 0–192 h (8 d), cells were washed extensively with PBS and lysed by scraping in 25 mM potassium phosphate buffer (pH 6.5, supplemented with 0.1 % (v/v) Triton X-100 and protease inhibitor cocktail (Roche)). Protein concentrations were determined and 10 μ g total protein (20 μ L) was denatured with 5 \times Laemmli buffer (50 % (v/v) 1M Tris-HCl, pH 6.8, 50 % (v/v) 100 % glycerol, 10 % (w/v) DTT, 10 % (w/v) SDS, 0.01 % (w/v) bromophenol blue), boiled for 4 min at 100 °C, and separated by electrophoresis on 7.5 % (w/v) SDS-PAGE gel running continuously at 90 V^{31,32,41}. Wet slab-gels were scanned on fluorescence using the Typhoon Variable Mode Imager (Amersham Biosciences) using λ_{EX} 488 nm and λ_{EM} 520 nm (band pass filter 40 nm) for green fluorescent imidate ABP 2 and β -epoxide ABP 4 and λ_{EX} 532 nm and λ_{EM} 610 nm (band pass filter 30 nm) for red fluorescent β -epoxide ABP 5. ABP-emitted fluorescence was quantified using ImageJ software (NIH, Bethesda, USA), and verified in-gel by presence of 50 femtomol equimolar green β -epoxide ABP 4– and red ABP 5-labeled imiglucerase. After fluorescence scanning, SDS-PAGE gels were fixed (50/40/10 – MeOH/H₂O/HAc) for 1 h, stained for total protein (50/40/10 with 1 % (w/v) CBB-G250) and de-stained (45/45/10). Coomassie brilliant blue-stained gels were scanned on a flatbed scanner.

Determination of *in situ* IC₅₀.

Confluent human skin control fibroblasts with wild-type GBA were incubated with 0–100 μ M IFG 1, 0–10 μ M imidate ABP 2 or 0–100 nM β -epoxide ABP 4 for 2 h at 37 °C and subsequently GBA-associated β -glucosidase activity was determined by incubation in the presence or absence of 250 μ M fluorescein-di- β -D-glucopyranoside (FDG) for 1 h at 37 °C. Next, cells were suspended by trypsinization, fixed in 3 % (w/v) *p*-formaldehyde and analyzed by FACS using FACS Calibur (BD Biosciences), FL1 channel (λ_{EX} 488 nm). In case of reversible inhibitor 1, all the procedures, including washing with PBS, occurred in the presence of 1 in the corresponding concentration as employed during the *in situ* incubation.

Pulse-chase of exogenous GBA.

rGBA (imiglucerase, 50 μ M) was incubated with (out) 100 μ M ABP 4 for 1 h in 150 mM Mcllvaine buffer, pH 5.2, supplemented with 0.2 % (w/v) sodium taurocholate and 0.1 % (v/v) Triton X-100), and at 37 °C, cleaned three times over a 30 kDa cutoff-filter with PBS. Mature human monocyte-derived macrophages were incubated with 300 μ M 3 for 2 h, hereafter cells were washed extensively with PBS, incubated with 100 nM rGBA (control) or 4-labeled rGBA with for 30 minutes at 37 °C, again washed extensively and medium refreshed. After 0–48 h,

cells were again washed extensively with PBS and lysed by scraping in 25 mM potassium phosphate buffer (pH 6.5, supplemented with 0.1 % (v/v) Triton X-100 and protease inhibitor cocktail (Roche)). Protein concentrations were determined in the lysates and, of the control rGBA-treated cells, 10 μ g total protein was labeled *in vitro* with 1 μ M β -epoxide ABP 4 in Mcllvaine buffer, pH 5.2 and with supplements, for 1 h at 37 °C. Finally, samples were denatured and 4-labeled proteins visualized by fluorescence scanning of the SDS-PAGE slab-gels. ABP-emitted fluorescence was quantified using ImageJ software (NIH, Bethesda, USA), *vide supra*.

Pulse-chase of GBA in living animals.

The appropriate ethics committee for animal experiments approved all experimental procedures. C57Bl/6J mice were obtained from Charles River (Wilmington, MA, USA) and fed a commercially available lab diet (CRM(E), Special Diet Services, UK). Two male C57Bl/6J mice were injected intravenously *via* tail vein with a single dose of 100 μ L PBS, four were injected with 100 μ L PBS containing 100 picomoles ABP 4 ($\sim 2 \mu$ g kg⁻¹) six weeks prior sacrifice, and four mice received the same dose every 48 hours for 15 days prior sacrifice. At termination of the experiment, the mice were anesthetized with FFM mix (25/25/50 fentanyl/citrate/midazolam/H₂O) then perfused *via* the heart into the aortic root with PBS, flowing at 3.0 mL min⁻¹, by using a syringe pump (Harvard apparatus, Holliston, MA, USA). The liver was collected and directly frozen in liquid nitrogen. Homogenates were made in 25 mM potassium phosphate buffer, pH 6.5, supplemented with 0.1 % (v/v) Triton X-100 and ABP 4-labeled GBA in 10 μ g total protein was analyzed *via* SDS-PAGE. After fluorescence scanning, SDS-PAGE gels were fixed and stained with CBB, *vide supra*.

Pulse-chase of normal and Gaucher patient skin fibroblasts.

Confluent human skin fibroblasts homozygous for wild-type, N370S or L444P GBA were cultured with medium supplemented with 100 nM ABP 5, 100 μ M leupeptin or both components. Medium was completely refreshed every fortnight, and after 0–12 days cells were lysed by scraping in 25 mM potassium phosphate buffer (pH 6.5, supplemented with 0.1 % (v/v) Triton X-100 and protease inhibitor cocktail (Roche)). After determination of the protein concentration, 10 μ g total protein was incubated with 100 nM ABP 4 (if fibroblasts were not treated by β -epoxide ABP 5 *in situ*), dissolved in 150 mM Mcllvaine buffer (pH 5.2, supplemented with 0.2 % (w/v) sodium taurocholate, 0.1 % (v/v) Triton X-100 and protease inhibitor cocktail (Roche)) for 1 h at 37 °C. Finally, samples were analyzed by SDS-PAGE on two gels: one for fluorescence scanning followed by CBB staining, and one for Western blotting; this was accomplished by transfer of the protein for 1 h at 12 V, followed by blocking of the membrane with 2 % (w/v) BSA in TBST buffer (50 mM Tris-HCl, pH 7.4, 150 mM NaCl, 0.1 % (v/v) Tween-20), overnight treatment with 1:1,000 diluted primary mouse α -human GBA mAb (8E4, 2 % (w/v) BSA in TBST), washing with TBST for 20 min (repeated 6 times), followed by 1:10,000 diluted secondary rabbit α -mouse IRD680 (Cell Signaling, 2 % (w/v) BSA in TBST), subsequent washing with TBST for 20 min (repeated 6 times), and read-out on an

Odyssey infrared scanner (Licor). Fluorescence emitted by either ABP-labeled proteins or antibodies was quantified using ImageJ software (NIH, Bethesda, MD, USA), *vide supra*.

In situ treatment with IFG 1 or imidate 2.

Confluent human skin fibroblasts homozygous for wild-type, N370S or L444P GBA were incubated for 12 days with 100 nM ABP 5, 100 μM leupeptin, both, or with 0.001–100 μM IFG 1 or imidate 2. Medium was completely refreshed every fortnight, and samples were treated as described earlier, *vide supra*.

Acknowledgments

This work was supported by The Netherlands Organization for Scientific Research (NWO-CW ChemThem "Chemical biology of glucosylceramide metabolism") and the European Research Council (ERC) (ERC AdvGr CHEMBIOSPHING).

Conflict of interest

None declared.

References

1. Brady, R. O., Kanfer, J. N., Bradley, R. M. & Shapiro, D. Demonstration of a deficiency of glucocerebrosidase-cleaving enzyme in Gaucher's disease. *J. Clin. Invest.* **45**, 1112–1115 (1966).
2. Patrick, A. A deficiency of glucocerebrosidase in Gaucher's disease. *Biochem J.* **97**, 17C–18C (1965).
3. Berg-Fussman, A., Grace, M. E., Ioannou, Y. & Grabowski, G. A. Human acid beta-glucosidase. N-glycosylation site occupancy and the effect of glycosylation on enzymatic activity. *J. Biol. Chem.* **268**, 14861–6 (1993).
4. Reczek, D. *et al.* LIMP-2 Is a Receptor for Lysosomal Mannose-6-Phosphate-Independent Targeting of β-Glucocerebrosidase. *Cell* **131**, 770–783 (2007).
5. Zunke, F. *et al.* Characterization of the complex formed by β-glucocerebrosidase and the lysosomal integral membrane protein type-2. *Proc. Natl. Acad. Sci.* **113**, 3791–3796 (2016).
6. Aerts, J. M. *et al.* Glucocerebrosidase, a lysosomal enzyme that does not undergo oligosaccharide phosphorylation. *Biochim. Biophys. Acta* **964**, 303–8 (1988).
7. Saftig, P. & Klumperman, J. Lysosome biogenesis and lysosomal membrane proteins: trafficking meets function. *Nat. Rev. Mol. Cell Biol.* **10**, 623–635 (2009).
8. Dvir, H. *et al.* X-ray structure of human acid-β-glucosidase, the defective enzyme in Gaucher disease. *EMBO Rep.* **4**, 704–709 (2003).
9. Lieberman, R. L. A Guided Tour of the Structural Biology of Gaucher Disease: Acid-β-Glucosidase and Saposin C. *Enzyme Res.* **2011**, 973231 (2011).
10. Brumshtein, B. *et al.* Crystal structures of complexes of N-butyl- and N-nonyl-deoxynojirimycin bound to acid beta-glucosidase: insights into the mechanism of chemical chaperone action in Gaucher disease. *J. Biol. Chem.* **282**, 29052–8 (2007).
11. E. Beutler, G. A. G. in *C.R. Scriver, W.S. Sly, D. Valle (Eds.), The Metabolic and Molecular Bases of Inherited Disease, 8th ed.* 3635–3668 (McGraw-Hill, New York, 2001).
12. Hruska, K. S., LaMarca, M. E., Scott, C. R. & Sidransky, E. Gaucher disease: mutation and polymorphism spectrum in the glucocerebrosidase gene (GBA). *Hum. Mutat.* **29**, 567–583 (2008).
13. Tan, Y. L. *et al.* ERdj3 is an endoplasmic reticulum degradation factor for mutant glucocerebrosidase variants linked to Gaucher's disease. *Chem. Biol.* **21**, 967–76 (2014).
14. Schmitz, M., Alfalah, M., Aerts, J. M. F. G., Naim, H. Y. & Zimmer, K.-P. Impaired trafficking of mutants of lysosomal glucocerebrosidase in Gaucher's disease. *Int. J. Biochem. Cell Biol.* **37**, 2310–20 (2005).
15. Wei, R. R. *et al.* X-ray and Biochemical Analysis of N370S Mutant Human Acid - Glucosidase. *J. Biol. Chem.* **286**, 299–308 (2011).
16. van Weely, S. *et al.* Role of pH in determining the cell-type-specific residual activity of glucocerebrosidase in type 1 Gaucher disease. *J. Clin. Invest.* **91**, 1167–75 (1993).
17. Sawkar, A. R. *et al.* Chemical chaperones increase the cellular activity of N370S beta - glucosidase: a therapeutic strategy for Gaucher disease. *Proc. Natl. Acad. Sci. U. S. A.* **99**, 15428–33 (2002).
18. Grace, M. E., Graves, P. N., Smith, F. I. & Grabowski, G. A. Analyses of catalytic activity and inhibitor binding of human acid beta-glucosidase by site-directed mutagenesis. Identification of residues critical to catalysis and evidence for causality of two Ashkenazi Jewish Gaucher disease type 1 mutations. *J. Biol. Chem.* **265**, 6827–35 (1990).
19. Ohashi, T. *et al.* Characterization of human glucocerebrosidase from different mutant alleles. *J. Biol. Chem.* **266**, 3661–7 (1991).
20. Jonsson, L. M. V *et al.* Biosynthesis and maturation of glucocerebrosidase in Gaucher fibroblasts. *Eur. J. Biochem.* **164**, 171–179 (1987).
21. Ferraz, M. J. *et al.* Gaucher disease and Fabry disease: New markers and insights in pathophysiology for two distinct glycosphingolipidoses. *Biochim. Biophys. Acta - Mol. Cell Biol. Lipids* **1841**, 811–825 (2014).
22. Dekker, N. *et al.* Elevated plasma glucosylsphingosine in Gaucher disease: relation to phenotype, storage cell markers, and therapeutic response. *Blood* **118**, e118–e127 (2011).
23. Siebert, M., Sidransky, E. & Westbroek, W. Glucocerebrosidase is shaking up the synucleinopathies. *Brain* **137**, 1304–1322 (2014).
24. Barton, N. W. *et al.* Replacement therapy for inherited enzyme deficiency--macrophage-targeted glucocerebrosidase for Gaucher's disease. *N. Engl. J. Med.* **324**, 1464–70 (1991).
25. Desnick, R. J. & Schuchman, E. H. Enzyme Replacement Therapy for Lysosomal Diseases: Lessons from 20 Years of Experience and Remaining Challenges. *Annu. Rev. Genomics Hum. Genet.* **13**, 307–335 (2012).
26. Zechel, D. L. *et al.* Iminosugar Glycosidase Inhibitors: Structural and Thermodynamic Dissection of the Binding of Isofagomine and 1-Deoxynojirimycin to β-Glucosidases. *J. Am. Chem. Soc.* **125**, 14313–14323 (2003).
27. Steet, R. A. *et al.* The iminosugar isofagomine increases the activity of N370S mutant

- acid beta-glucosidase in Gaucher fibroblasts by several mechanisms. *Proc. Natl. Acad. Sci. U. S. A.* **103**, 13813–8 (2006).
28. Benito, J. M., García Fernández, J. M. & Ortiz Mellet, C. Pharmacological chaperone therapy for Gaucher disease: a patent review. *Expert Opin. Ther. Pat.* **21**, 885–903 (2011).
 29. Jung, O., Patnaik, S., Marugan, J., Sidransky, E. & Westbroek, W. Progress and potential of non-inhibitory small molecule chaperones for the treatment of Gaucher disease and its implications for Parkinson disease. *Expert Rev. Proteomics* **13**, 471–9 (2016).
 30. Walvoort, M. T. C. *et al.* Tuning the leaving group in 2-deoxy-2-fluoroglucoside results in improved activity-based retaining β -glucosidase probes. *Chem. Commun.* **48**, 10386–10388 (2012).
 31. Li, K.-Y. *et al.* Synthesis of Cyclophellitol, Cyclophellitol Aziridine, and Their Tagged Derivatives. *European J. Org. Chem.* **2014**, 6030–6043 (2014).
 32. Kallemeijn, W. W. *et al.* Novel activity-based probes for broad-spectrum profiling of retaining β -exoglucosidases in situ and in vivo. *Angew. Chemie - Int. Ed.* **51**, 12529–12533 (2012).
 33. Abian, O. *et al.* Therapeutic strategies for Gaucher disease: miglustat (NB-DNJ) as a pharmacological chaperone for glucocerebrosidase and the different thermostability of velaglucerase alfa and imiglucerase. *Mol. Pharm.* **8**, 2390–7 (2011).
 34. Lieberman, R. L., D'aquino, J. A., Ringe, D. & Petsko, G. A. Effects of pH and iminosugar pharmacological chaperones on lysosomal glycosidase structure and stability. *Biochemistry* **48**, 4816–27 (2009).
 35. LASCH, J., BESSMERTNAYA, L., KOZLOV, L. V. & ANTONOV, V. K. Thermal Stability of Immobilized Enzymes Circular Dichroism, Fluorescence and Kinetic Measurements of alpha-Chymotrypsin Attached to Soluble Carriers. *Eur. J. Biochem.* **63**, 591–598 (1976).
 36. Qi, X. & Grabowski, G. A. Acid β -Glucosidase: Intrinsic Fluorescence and Conformational Changes Induced by Phospholipids and Saposin C[†]. *Biochemistry* **37**, 11544–11554 (1998).
 37. MITCHELL, S. A Photo-electric Method for Measuring Circular Dichroism. *Nature* **166**, 434–435 (1950).
 38. Kim, J. H., Sumranjit, J., Kang, H. J. & Chung, S. J. Discovery of coumarin derivatives as fluorescence acceptors for intrinsic fluorescence resonance energy transfer of proteins. *Mol. Biosyst.* **10**, 30–33 (2014).
 39. Celej, M. S., Montich, G. G. & Fidelio, G. D. Protein stability induced by ligand binding correlates with changes in protein flexibility. *Protein Sci.* **12**, 1496–1506 (2003).
 40. Van Weely, S. *et al.* Function of oligosaccharide modification in glucocerebrosidase, a membrane-associated lysosomal hydrolase. *Eur. J. Biochem.* **191**, 669–77 (1990).
 41. Witte, M. D. *et al.* Ultrasensitive in situ visualization of active glucocerebrosidase molecules. *Nat. Chem. Biol.* **6**, 907–913 (2010).
 42. Aerts, J. M. *et al.* The occurrence of two immunologically distinguishable beta-glucocerebrosidases in human spleen. *Eur. J. Biochem.* **150**, 565–74 (1985).
 43. Aerts, J. M. *et al.* A procedure for the rapid purification in high yield of human glucocerebrosidase using immunoaffinity chromatography with monoclonal antibodies. *Anal. Biochem.* **154**, 655–63 (1986).
 44. Jung, O., Patnaik, S., Marugan, J., Sidransky, E. & Westbroek, W. Progress and potential of non-inhibitory small molecule chaperones for the treatment of Gaucher disease and its implications for Parkinson disease. *Expert Rev. Proteomics* **13**, 471–479 (2016).
 45. Maegawa, G. H. B. *et al.* Identification and Characterization of Ambroxol as an Enzyme Enhancement Agent for Gaucher Disease. *J. Biol. Chem.* **284**, 23502–23516 (2009).
 46. Babajani, G., Tropak, M. B., Mahuran, D. J. & Kermodé, A. R. Pharmacological chaperones facilitate the post-ER transport of recombinant N370S mutant β -glucocerebrosidase in plant cells: evidence that N370S is a folding mutant. *Mol. Genet. Metab.* **106**, 323–9 (2012).
 47. Zimran, A., Altarescu, G. & Elstein, D. Pilot study using ambroxol as a pharmacological chaperone in type 1 Gaucher disease. *Blood Cells, Mol. Dis.* **50**, 134–137 (2013).
 48. Bendikov-Bar, I., Maor, G., Filocamo, M. & Horowitz, M. Ambroxol as a pharmacological chaperone for mutant glucocerebrosidase. *Blood Cells. Mol. Dis.* **50**, 141–5 (2013).
 49. Narita, A. *et al.* Ambroxol chaperone therapy for neuronopathic Gaucher disease: A pilot study. *Ann. Clin. Transl. Neurol.* **3**, 200–215 (2016).
 50. Yadav, A. K. *et al.* Fluorescence-quenched substrates for live cell imaging of human glucocerebrosidase activity. *J. Am. Chem. Soc.* **137**, 1181–9 (2015).
 51. Fontana, A. *et al.* Probing protein structure by limited proteolysis. *Acta Biochim. Pol.* **51**, 299–321 (2004).
 52. Liou, B. *et al.* Analyses of variant acid beta-glucosidases: effects of Gaucher disease mutations. *J. Biol. Chem.* **281**, 4242–53 (2006).
 53. Miocić, S. *et al.* Identification and functional characterization of five novel mutant alleles in 58 Italian patients with Gaucher disease type 1. *Hum. Mutat.* **25**, 100 (2005).
 54. Neumann, J. *et al.* Glucocerebrosidase mutations in clinical and pathologically proven Parkinson's disease. *Brain* **132**, 1783–94 (2009).
 55. Grace, M. E., Desnick, R. J. & Pastores, G. M. Identification and expression of acid beta-glucosidase mutations causing severe type 1 and neurologic type 2 Gaucher disease in non-Jewish patients. *J. Clin. Invest.* **99**, 2530–7 (1997).
 56. Ben Bdira, F. *et al.* Hydrophobic Interactions Contribute to Conformational Stabilization of Endoglycoceramidase II by Mechanism-Based Probes. *Biochemistry* **55**, 4823–35 (2016).
 57. Rempel, B. P., Tropak, M. B., Mahuran, D. J. & Withers, S. G. Tailoring the specificity and reactivity of a mechanism-based inactivator of glucocerebrosidase for potential therapeutic applications. *Angew. Chem. Int. Ed. Engl.* **50**, 10381–3 (2011).

Supplemental data

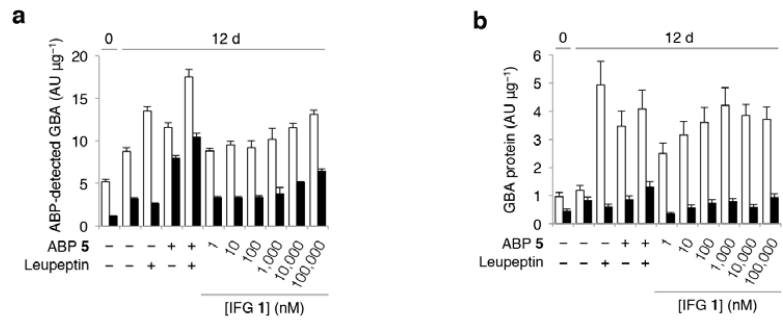


Figure S1. *In situ* GBA stabilization by IFG. Wild-type GBA (*open columns*) and N370S GBA (*closed columns*) fibroblasts were grown for 12 days in the absence or presence of incubated with leupeptin, ABP 5, both, or 0.001–100 μM IFG 1. **(a)** Quantification of ABP-emitted fluorescence from *in vitro* ABP 4-labeled controls, leupeptin- and IFG 1-treated cells, compared to fluorescence of *in situ* ABP 5-labeled GBA. **(b)** Quantification of GBA peptide after treatment. All data expressed as average of $n = 2$, \pm SD.

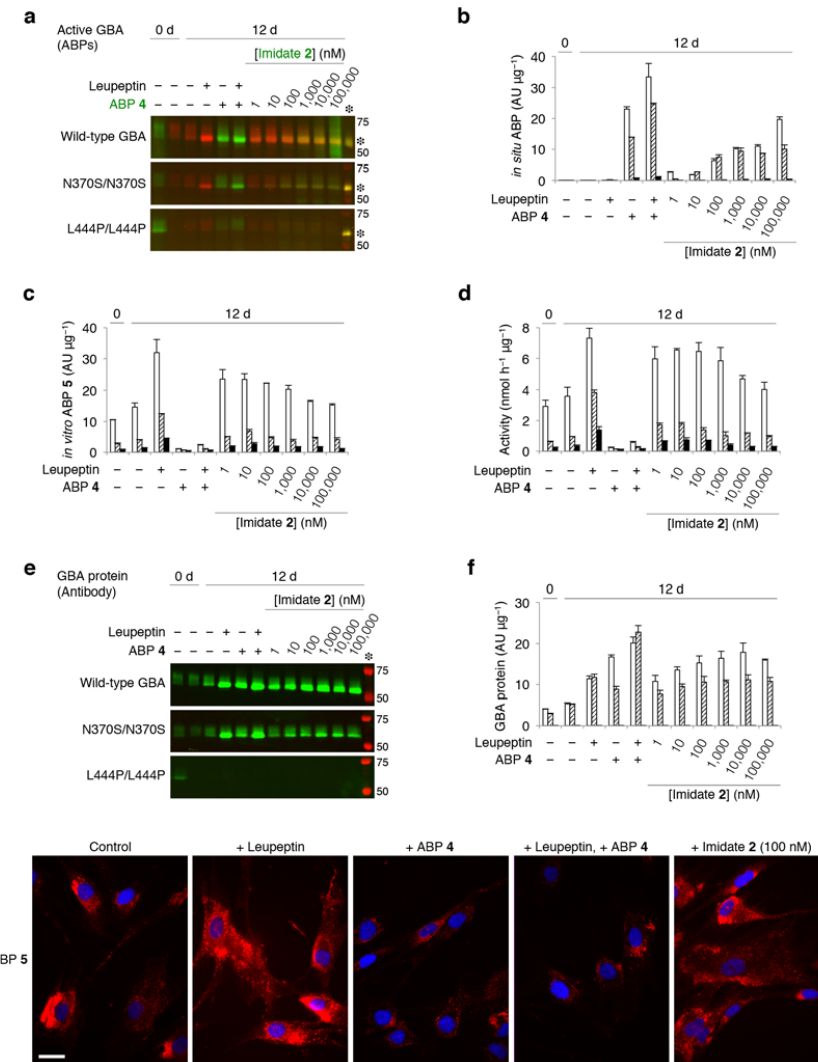


Figure S2. *In situ* stabilization of GBA by imidate 2. (a) Wild-type (*top*), N370S (*middle*) and L444P GBA (*bottom row*) Gaucher patient fibroblasts were grown for 12 days in the absence or presence of leupeptin, green β -epoxide 4, both, or 0.001–100 μM green imidate 2. Gel depicts *in situ* labeling of active GBA by imidate 2 or β -epoxide 4 followed by *in vitro* labeling of residual active GBA molecules with excess red ABP 5. Equal green- and red fluorescence yields yellow overlay; fluorescence calibrated with 50 fmol equimolar ABP 4- and 5-labeled imiglucerase present on each SDS-PAGE gel (*asterisk*). (b) Quantification of *in situ* GBA labeling by imidate 2 or ABP 4, with wild-type (*white columns*), N370S (*dashed columns*) and L444P (*black*) fibroblasts. (c) Quantification of *in vitro* labeling of residual active GBA molecules with excess ABP 5. (d) Residual GBA-associated β -glucosidase activity. (e) Detection of GBA protein (*green*) by Western immunoblotting of gels depicted in a (molecular weight ladder in *red*) of fibroblasts with wild-type (*top*), N370S (*middle*) and L444P GBA (*bottom row*),

after aforementioned treatments, *vide supra*. (f) Quantification of GBA protein levels. Data expressed as mean of duplicate quantifications \pm SD. (g) Fluorescence micrographs depicting red-fluorescent ABP 5-labeling of residual active N370S GBA molecules in GD patient fibroblasts. From *left to right*: cells grown for 12 days in absence of additives, with leupeptin, with 100 nM green fluorescent ABP 4, both, or with 100 nM imidate 2. GBA was post-labeled for 2 h with 10 nM ABP 5. Scale-bar represents 25 μ m. All data expressed as average of $n = 2$, \pm SD.

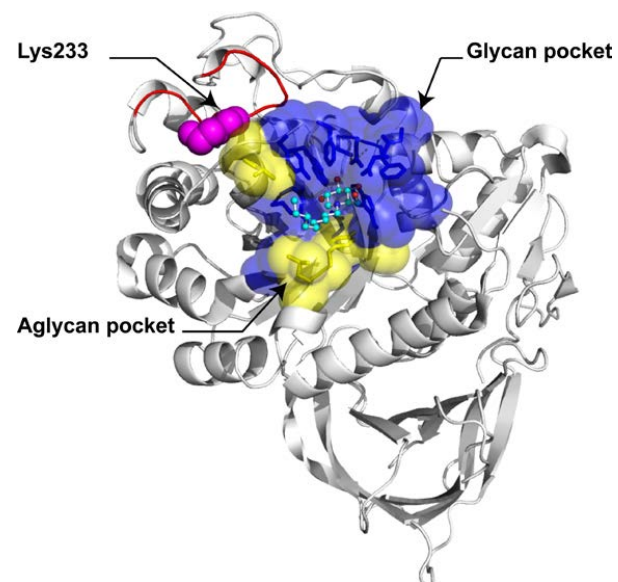


Figure S3. GBA structure and the trypsin cutting site.

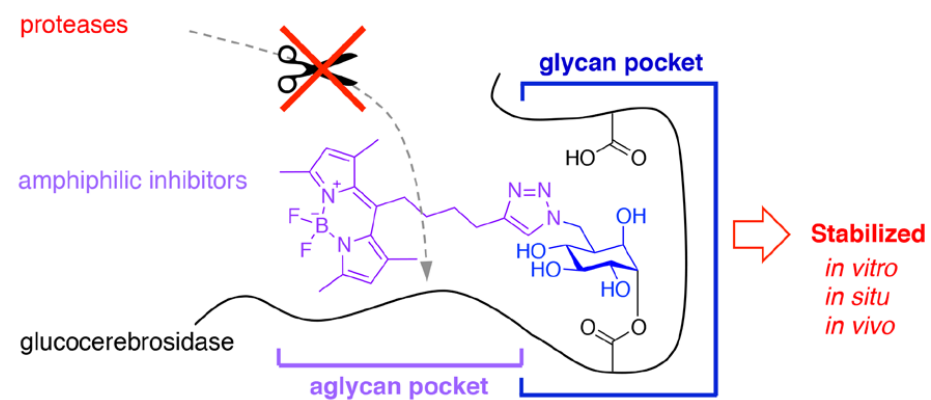


Figure S4. Proposed graphical abstract.